Romanian Reports in Physics, Vol. 64, No. 2, P. 467–481, 2012

DROP IMAGES WITH REFLECTION SPOTS: IMPROVED PROCESSING FOR DETERMINATION OF WETTING CONTACT ANGLES

V.F. COTOROBAI

National Institute of Materials Physics, P.O. Box MG-07, R-077125 Magurele, Romania,
E-mail: cotorobai.florin@infim.ro

Received March 25, 2011

Abstract. Improvements in automatic processing of movie frames taken on commercial Drop Shape Analysis systems are presented, regarding the use of particular edge detection algorithms that account for optical peculiarities of the drop image formed on digital video camera sensors. These improvements can lead to better measurements of contact angles for drop images that present spots of reflected light close to edge and in the case of very low contact angles.

Key words: Contact angle, sessile drop, edge detection, collimated back-lighting, reflection.

1. INTRODUCTION

The tensiometric methods for characterization of liquids, that analyze the drop shape [1–3] are often preferred when measuring wetting contact angles, due to a large choice of instruments available on the market, their relative simplicity in use and because they need small quantities of analyzed liquid (micro-liters). The instruments extracting the wetting information from the shape of drop images – contact angle goniometers (CAGs) – have a digital video camera focused on a drop of studied liquid, lying on a flat, horizontal surface made of material whose wetting is measured, against a bright background. Under proper conditions of lens focus, camera contrast, gain and exposure settings and background lighting level, the video frames present a nearly black silhouette of the drop on a uniform-lit background, with a sharp transition from dark to bright on the drop contour.

The digitized images from video camera are processed to identify points on this transition region and thus define the contour of the drop image. If a sufficient number of such points are found, and a base line can be identified on the picture, then the drop shape is approximated with a smooth curve and contact angles can be calculated in the points where the curve intersects the base line. The baseline is a roughly horizontal line defined by two points on sides of the drop image, where drop contour is touching the surface of the support.

The application software associated with CAGs typically uses gradient-based [4–6] or image entropy [7] edge detection algorithms that essentially locate points with steepest variation of pixel brightness across the contour, after performing some sort of filtration (smoothing) of the image. Any procedure looking for variation of pixel brightness is a differential operator and therefore will be affected by the image noise. The smoothing of the image is a low-pass filter meant to reduce the influence of the pixel noise or of the dust particles that can be present on the surface of drop or of the support material. These algorithms will be further noted SVED, from steepest variation edge detectors. SVED were developed in the general context of image processing and the dependence of their performance and errors on the image noise and camera settings is well understood [3, 8]. Nevertheless their performance is most often defined or compared with respect to an ideal image and less attention is paid to physics of its formation from the originating object subjected to lighting.

For drop images taken with correct settings of camera and lighting as noted before, the SVED methods are fast and produce reliable results. In industrial practice, when some of these pre-requisites are not fully satisfied, e.g. due to operator overlook, insufficient preparation or sample peculiarities, one is left with images of lower quality, that result in bigger measurement errors, incorrect estimations, or in important rates of movie frame rejection. These images can have low contrast, insufficiently sharp drop profile (out of focus) or contain parasitic light reflections on drop surface that lead to important errors or failure of edge detection algorithms. The light reflection spots on drop surface can induce particularly important alterations on the results of SVED algorithms because these methods assume that the profile of brightness transition on images of objects with edges depends only of camera focus, the quality of the optical system and the noise of sensor, ignoring the influence of reflected light on detected edges. The evolution of commercial CAGs available on the market last years is mainly driven by hardware improvements as higher resolution or speed of camera sensors, or various options offered for back-lighting or drop feeding. The basic algorithmic features of software accompanying the instruments are extensively treated in the review [3] and generally it evolves slower, compared with improvements of the hardware.

The paper considers the case of images produced using the method of sessile drop to measure the contact angles and illustrates proposed processing improvements. The pictures produced by a commercial CAG were processed with LabVIEW programs developed for this purpose and compared with results produced by the software provided by the manufacturer of the instrument.

2. EQUIPMENT SETTINGS THAT INFLUENCE IMAGE QUALITY

The majority of CAGs in use have black-and-white interlaced digital video cameras with 8 bit digital acquisition that produce still images or movies at around

25 fps, that are further processed with the associated software. The term “interlaced video” means that, in order to reduce the cost (and performance) of electronics involved in transmission of image from camera sensor to processing computer, one registers and transmits first the odd rows of the image (odd field), then the even rows forming the corresponding field. On the computer acquiring the video, the full frames have to be assembled subsequently, by merging odd and even fields [9]. Newer instruments can offer better alternatives as progressive scan cameras working at high frame rates, but those and related frame grabbers are still notably more expensive and thus less frequent in typical industry labs. For purposes of drop shape analysis it is important to set correctly the gain, contrast and the level of back-lighting to use the full range of Analog to Digital Conversion (ADC) electronics and avoid saturation effects that can lead to incorrect work of edge finding algorithms. In absence of saturation, the brightness of pixels corresponding to the illuminated background on the image has a random noise of a few ADC counts.

When measuring the advancing or receding angles by using the method of embedded needle with normal speed (25–60 fps) interlaced video cameras, it happens often to find images that contain characteristic artifacts due to the electronics of image acquisition. These artifacts can appear as jagged contours (see Fig. 1) of the drop image or even ghost images (as shown in Fig. 2), if the picture was taken in a moment of fast movement of drop surface. The drop surface can move or change the shape very fast when the contact line of the drop overcomes a pinning point on the support surface or during separation from tip of the needle. In these situations, characteristic times of movement can be much shorter than factory setting for camera shutter. The odd and even fields of a given movie frame (right side of Fig. 2) being taken at different moments of time, they contain visually distinct information and produce “ghostly” frames when merged. This effect can be eliminated or reduced by taking shorter values for the shutter duration (with a corresponding increase of the lighting or camera gain), or by replacing the standard back-lighting system with a stroboscopic one [10, 11] and using external triggering for camera, if available.

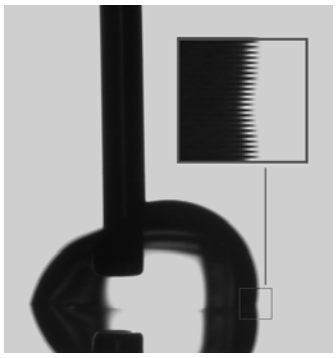

Fig. 1 – Jagged profile due to fast motion.

Inappropriate back-lighting can cause light to reflect on the surface of the drop oriented towards the camera, that appear as lighter spots on the drop profile, often very close to its boundaries. Such spots can affect the work of edge-finding routines that will fail or deliver results with increased errors. This influences the estimated contact angles, especially in situations of drops with distorted shape, when contact angles at left and right of drop image have to be computed separately. This is the case for drops in contact with pumping needle, or sitting on surfaces with inhomogeneous or anisotropic wetting properties, when a theoretical shape for the drop image contour does not exist.

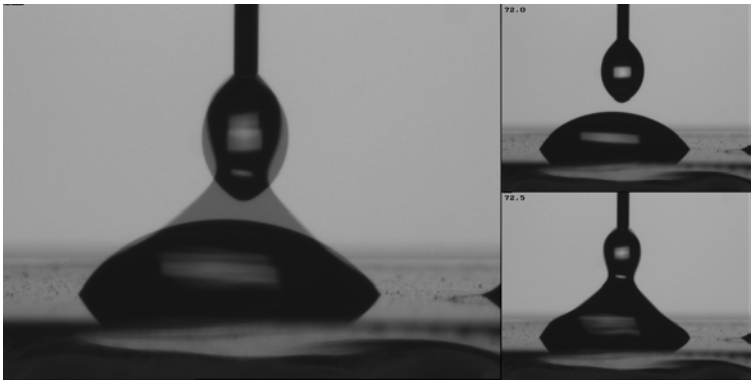

Fig. 2 – Ghost images: left – full interlaced frame; right – odd (up) and even (down) fields of the frame.

We will make a geometrical optics analysis of light reflected by drop surface, assuming a spherical drop and using the drawing and notations of Fig. 3.

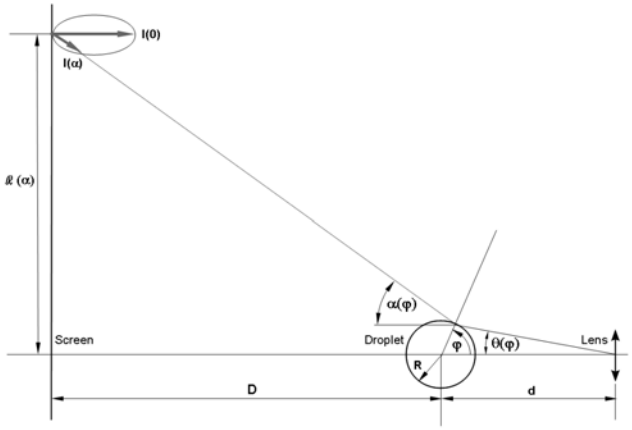

Fig. 3 – Geometry of light ray trajectories in a contact angle goniometer**:** The drop is represented as a sphere with radius *R*. On the left side there is the screen. The light comes from the left side and reflects on the drop surface towards the lens on the right side.

In this drawing the rays emitted from a point situated on the vertical screen at left, at the distance $\Re(\alpha)$ from the optical axis of the lens, enter the lens at an angle $\theta(\varphi)$, if reflected by the drop surface in a point whose radius makes the angle φ with optical axis of the camera lens. The quantities D and d are the distances from drop center to the back-lighting screen and to camera lens respectively and R is the drop radius. The back-lighting screen is assumed to produce a diffuse illumination having the intensity $I(0)$ on a direction normal to screen surface and $I(\alpha)$ on a direction making an angle α with the normal to screen. In our case the angle α depends on φ thus one has $\Re(\alpha(\varphi))$ and $I(\alpha(\varphi))$.

One obtains thus the formulas

$$\tan(\theta(\varphi)) = \frac{\tan\varphi}{(d'/\cos\varphi - 1)}, \tag{1}$$

$$\tan(\alpha(\varphi)) = \frac{(-d'\sin 2\varphi + \sin\varphi)}{(d'\cos 2\varphi - \cos\varphi)}, \tag{2}$$

and

$$\Re(\alpha(\varphi)) = R[\sin\varphi + (D' + \cos\varphi)\tan\alpha(\varphi)], \tag{3}$$

where $d' = d / R >> 1$ and $D' = D/R >> 1$. The angle φ can vary from the maximum value $\varphi_{max} = \arccos(1/d')$ to a minimum value φ_∞, which is the first quadrant angle corresponding to the positive root of equation

$$d'\cos(2\varphi_\infty) - \cos(\varphi_\infty) = 0, \tag{3}$$

where $\varphi_\infty \approx \pi/4 - \delta - \delta^2$ and $\delta = 1/(2\sqrt{2}d')$. The minimum angle φ_∞ corresponds to an infinite back-lighting screen. In a real device, ignoring the presence of stray light originating from outside of the back-lighting system, the minimum angle φ_{min} is limited by the dimensions of back-lighting screen, that in Fig. 3 correspond to $\Re(\alpha)$; one has $\varphi_{max} > \varphi_{min} > \varphi_\infty$.

One can see from the same drawing (Fig. 3) that the spots are caused by rays coming at large angles with respect to direction normal to the plane of lighting background, that enter the camera lens, after being reflected by drop surface. These rays originate from the margins of back-lighting screen or from outside the goniometer; therefore such spots, if present, can be reduced or eliminated by covering a fraction of outer area of illuminated background with some opaque material. An alternative possibility is using a parallel beam of light, as e.g. in ref. [12]. Without taking special precautions on restricting the illuminated area of the background, one can see a lighter region of the drop profile close to its border, so edge-finding algorithms can systematically underestimate the size of the drop image.

For a clearer illustration of this effect, the formulas (1–3) were used to calculate the profile of brightness variation across the image of a 3mm diameter perfectly reflecting sphere, placed in front of a back-lighting screen. The distances

from sphere to screen and to imaging lens were taken to correspond to a real contact angle goniometer and the image magnification was assumed to be 1:1. The influence of modulation transfer function (MTF) of the optical system [20], that causes some smoothing of sharp brightness transitions on the image, was neglected. The Fig. 4 shows the calculated profiles of brightness for a distribution of back-lighting of lambertian type (~ $\cos^2\theta$), for a more collimated one (~ $\cos^4\theta$), and for a black disk of same diameter. The edge of the image of black disk is absolutely sharp, whereas for diffuse back-lighting the transition of brightness is more gradual for less collimated lighting, extending toward the interior of the image of the sphere.

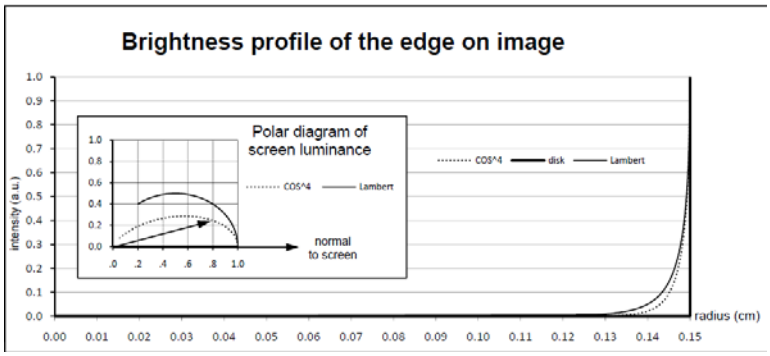

Fig. 4 – The dependence of brightness profile on lighting collimation, across the image of a reflecting sphere put in front of an illuminated screen.

This correlates with findings made in ref. [13–14]. When using an edge finding algorithm based on thresholding, authors of ref. [12] have found empirically that the threshold giving the best concordance between the estimated drop profile and that resulted from Laplace theory is $0.67(I_W - I_B)$. That means an edge shifted outwards from the centre of drop image, compared to value $0.5(I_W - I_B)$ suggested by generic edge finding algorithms. Here I_W and I_B are white (background) and black (interior of drop image) pixel brightness levels respectively.

3. METHODOLOGY

3.1. PROCESSING THE FRAMES WITH FAST MOVEMENT

During fast movement of drop surface the interlaced-video cameras produce frames where odd and even fields are visually different (being taken at different times of drop shape evolution). When combined in the resulting frame, the drop

profile will appear jagged, or even a superposition of two distinct drop shapes will appear in the frame. These frames are usually rejected by standard CAG software, or may need operator guiding, if software allows it.

If one splits the frame in component fields of odd and even pixel rows (see again Fig. 1), and interpolates in each field the missing rows by averaging the adjacent lines, one can process normally the drop profile, yet with the expense of somewhat bigger errors. Thus for a given frame one obtains two sets of contact angles, for odd and even fields, that correspond to two different moments of camera sensor exposition.

3.2. PROPOSED METHOD OF EDGE DETECTION

The choice of edge detection algorithms for processing of images provided by CAG is conditioned by specifics of these images: gray-scale, typically 8 bit deep and a low pixel noise of a few ADC counts. In this case, differential edge detectors are efficient and have a high accuracy [15].

These algorithms assume an object with a sharp edge, which produces a more or less neat image (limited by lens quality and focus setting) on camera sensor, which in turn samples it onto a bitmap. In this case, the points with greatest amount of the brightness change are an unbiased estimate of the position of object profile on the image. They are located in the middle of the interval of monotonic change of pixel brightness across the edge. This fact is not true when stray light enters the camera lens after being reflected by drop surface, as is discussed below.

The drops photographed with lighting setups typical for CAGs, present several peculiarities from the optical point of view, which for unfavorable back-lighting conditions may require modified edge-finding algorithms in order to obtain correct descriptions of drop profile. The drop surface is perfectly smooth and its reflectivity is described by Fresnel formulas for grazing to medium angles of incidence. This fact combined with the presence of a diffuse lighting from the flat background screen that most CAGs use, leads to a more gradual and asymmetric decrease of brightness across the edge of drop image, due to rays entering the camera lens aperture after being reflected on drop surface. On drop images taken with improper back-lighting this can be seen as a halo adjacent to drop edge, on its inner side.

Let us consider a nearly-spherical drop, viewed against a background that provides a uniform diffuse illumination. The brightness of an image pixel inside the visible contour of the drop will be proportional to the product of Fresnel reflectance of drop surface and the intensity of the background light emitted on the direction that corresponds to that pixel on camera light sensor. Here one takes into account the full ray path after being emitted from back-light screen through reflection on drop surface, camera lens traversal and until it hits the pixel of camera sensor. For most back-lighting systems, the last material left by light rays before

entering the goniometer is a sheet of white diffuser material. The polar distribution of luminance for these materials is close to an ellipse with the big axis normal to diffuser sheet plane, and hence it contributes to produce a narrow but significant halo, as shown in Figs. 3, 4. An additional contribution to this halo is made by light rays diffracted forward at the edge of sphere, as remarked also in ref. [16].

Another source of trouble are the spots of reflected light for drops with strongly distorted surface, due to the contact with the needle or to pinning points or other defects on the support surface. In such situations standard edge detection algorithms produce erroneous results or fail for an important part of drop profile, because the steepest fall of the brightness can be somewhere on the edge of reflection spot and not on the edge of drop image, as can be seen in Fig. 7b. In these situations, it is possible to recover an important fraction of images using a different edge finding method, exposed below.

We propose a method that in some points is close to dynamic thresholding exposed in ref. [6], accounting additionally for the presence of diffraction [17, 18]. Instead of taking the position of steepest change from light background to dark interior of bubble image, one identifies the contour of bubble image with first pixel dark enough to be assigned to the start of brightness fall, taking into account the possible presence of diffraction at edges of bubble image. Thus the edges found by other methods are re-defined, being shifted from the position of the maximum gradient of brightness change, to the start of the region where the change begins.

The method makes an edge sampling by following the change of the brightness of pixels along a line starting from outside the drop, on the illuminated background, and directed towards the interior of drop profile. It assumes that the average background brightness around drop image is locally uniform (varies slowly across the frame) and affected by a small (a few ADC counts) random pixel noise. The algorithm implemented here looks for a contiguous range of pixels with monotonic decrease of brightness. This range must be larger than a minimal width (in pixels) and integrated brightness drop across it – greater than some threshold value. If such a range is found, the estimated edge position is taken at the location of first pixel with brightness lower than a local threshold. The threshold is lower than local average of background by four standard deviations of pixel noise in the same region. The background average and RMS noise values are estimated on each scan line where the edge is searched for, on a region of several tens of pixels outside drop image. For images of sharp edges, this method gives an edge contour shifted outwards by roughly half-width of Edge Spread Function (ESF) of the imaging system – see e.g. [19, 20] – with respect to standard edge-finding algorithms. A shift of few pixels outwards for the estimated drop edge has a reduced influence on values of computed contact angles, but is not acceptable for pendant drop measurements, where the volume of the drop has to be determined accurately. Considering the image of a sessile drop of spherical shape sitting on a horizontal surface as shown in Fig. 5, the effect of this shift on the value of contact angle can be compensated with formula (5):

$$\alpha \approx \alpha' - \arctan\left(\frac{2h}{R} / \tan\alpha'\right). \tag{5}$$

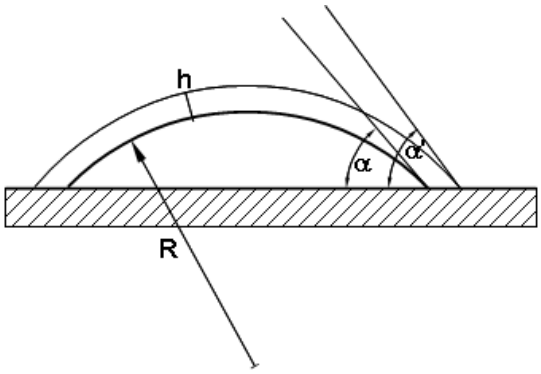

Fig. 5 – The effect of edge shift on estimated contact angle.

Here one assumes that the radius of the drop surface is R, the value of the edge shift caused by proposed algorithm is h, the real value of contact angle is α and the distorted one is noted with α'. In practical cases the edge shift h is less than 5 pixels, whereas R is in range from hundreds to thousands, thus the effect of edge shift is small, even for lowest measurable contact angles, that for CAGs are larger than ~4°.

For gray-scale drop images taken with 8-bit cameras in conditions of diffuse back-lighting, the first diffraction fringe can also be visible, as will be discussed next (see Fig. 6) and produce an additional shift, being slightly above pixel noise if camera settings avoid saturation. This shift can be corrected by lowering additionally the local threshold with the amplitude of the first diffraction minimum.

4. RESULTS

To evaluate the effect of un-collimated back-lighting on images of small reflective objects, a set of images of a (4.020 ± 0.003) mm rod of glass and a razor blade put aside on table of goniometer was used. The image of razor blade was used to determine ESF of the optical system and to estimate the intensity of the diffraction fringes. The images were taken in two conditions of lighting: standard illumination, corresponding to completely uncovered back-lighting screen, and collimated back-lighting, when lateral parts of the screen were covered, to avoid the rays emitted at large angles being reflected from rod surface. The central light strip visible on rod image in Fig. 6 is the image of the back-lighting screen as seen through the cylindrical lens represented by glass rod. The width of rod image was

sampled at 500 horizontal sections (adjacent rows) along rod height. The errors of the method resulted from the statistical treatment of these data. The profile of the brightness change across the edge of razor blade (the dark gray curve) was averaged over the same 500 rows, taking into account the slant of the edge. Its derivative, scaled for visibility – the light gray curve in Fig. 6 – shows the presence of faint diffraction fringes of first order.

The mean values of estimated width of rod image and its errors, in pixels, for standard and collimated illumination, for SVED and for the method proposed here are shown in Table 1. As expected, the estimated width of the rod image is smaller when back-lighting is less collimated.

One can see that SVED is more affected by non-collimated back-lighting than the algorithm proposed here, which instead gives an over-estimated rod diameter that is less dependent of back-lighting collimation. As noted before, the difference between values estimated with two methods is roughly 10 pixels and this corresponds to the width of ESF (plotted with dark gray in Fig. 6). The errors of edges

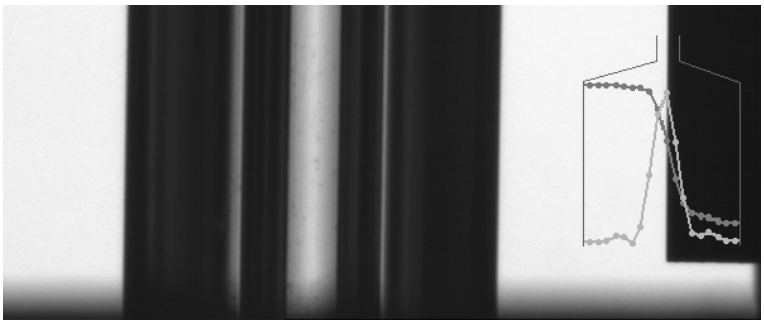

Fig. 6 – Glass rod (left) and razor blade (right) against a lit background. Overlaid are the brightness curve (dark gray) and its derivative (light gray), across the edge of razor blade**.**

Table 1

Estimated width of glass rod (in pixels) for compared methods

Illumination	Edge detection			
	SVED		proposed	
	width	error	width	error
un-collimated	370.2	0.25	380.1	2.6
collimated	370.9	0.24	380.6	1.6

estimated by SVED are notably smaller, because single-pixel noise is mediated for the number of pixels spanning the typical width of brightness transition region that defines edge. The proposed method has increased errors, because a sampling of the

edge is based on a pair of pixels only. For a knife-edge image produced by a system characterized by a given ESF, the edge sampling error by thresholding is roughly one third of quantity *NS* (noise spread) defined in [21]:

$$NS = \frac{\sqrt{2\pi} \cdot \sigma \cdot w}{ESF'(ESF^{-1}(\Theta))}, \tag{6}$$

where σ is the pixel noise RMS, Θ – the sampling threshold, and w – the width parameter of edge profile, if ESF is approximated with $(1/2)(\mathrm{erf}(x/\sqrt{2}w)+1)$ (x being the coordinate across the edge). The increased errors characteristic for edge detectors based on thresholding [22] can be still acceptable for evaluation of contact angles, if a sufficient number of samples along the edge are taken.

A further check of the proposed method was to process the images of a small plane-convex lens with known diameter and curvature radius of spherical surface. One can thus calculate the angle made by tangent to convex surface at its margin with the flat side of the lens (24.6° for the lens used) and compare it with the values found by a commercial DSA program and with proposed algorithm. In both cases, the contact angles were estimated as tangent to second degree polynomials drawn through points sampled on drop profile near contact line. Table 2 shows the values of the angle defined above, determined for left and right sides of the lens image.

Table 2

Estimated contact angles for a glass lens, for compared methods

Illumination	Edge detection			
	SVED		proposed	
	left side	right side	left side	right side
un-collimated	17.9°	17.8°	22.4°	23.9°
collimated	24.4°	25.2°	24.5°	26.0°

One can see that for contact angle measurements, the proposed method is less affected by the lack of collimation of back-lighting. Fig. 7 contains zoomed parts from graphic output windows of confronted software that show the effect of reflected light on edge detection and thus on estimated contact angles.

In Fig. 7 light gray is used for tangent lines and dark gray for edge points, for the proposed method. For the commercial software the tangent and edge points are white; the black points on profile show a smooth curve approximating locally the drop profile.

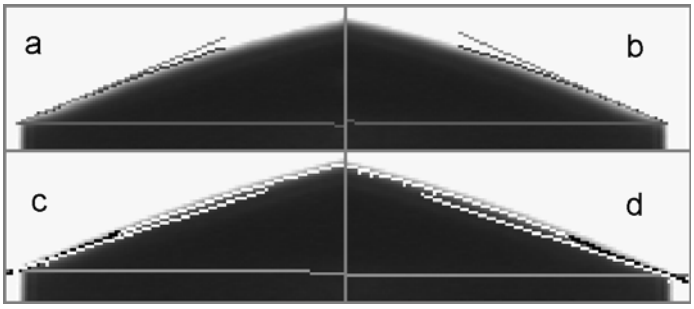

Fig. 7 – Influence of uncollimated lighting on estimated contact angles obtained with compared methods, for a test lens. The results of proposed algorithm are shown in the upper half of the picture. a, b – proposed method; c, d – commercial software.

For pictures with spots of reflected light close to the border of droplet image as shown in Fig. 8, the advantage of the proposed method is striking: whereas SVED – in the same commercial DSA program – squarely fails, our method is stable and gives contact angles close to correct values, albeit with bigger errors. The new method is particularly efficient in the case of drops contacting the pumping needle and for sessile drops deposed on strongly inhomogeneous or anisotropic substrates, when a parameterization for the whole drop profile is missing. In these situations only the parts of drop profile close to contact line give usable information for determination of contact angle, hence their accurate estimation is important.

The picture shown in Fig. 8 comes from a 350 frame video taken in rather poor lighting conditions. The video of a sessile drop sitting on a substrate with soluble components was used to study temporal evolution of contact angles. The proposed method for edge finding failed on 50 frames, whereas the software provided by the manufacturer of the goniometer discarded 245 frames. The last fact served actually as a stimulus to develop the method discussed in this paper.

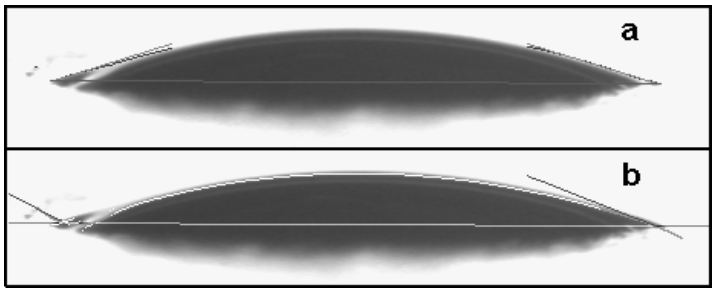

Fig. 8 – Influence of uncollimated lighting on estimated contact angles obtained with compared methods, for a test lens. The results of proposed algorithm are shown in the a): upper half of the picture; b) lower half shows the result of instrument's own software.

As the purpose of this comparison was the evaluation of the proposed edge detection method, the original DSA software of the goniometer was run to determine separately left and right contact angles, without making assumptions about the whole shape of the drop. The left and right-side contact angles obtained with both methods were confronted with more trustworthy values, used by approximating the drop profile with a circle (continuous curve on graph), which is a good approximation in our case. This approximation, which leads to equal values for left- and right contact angles for a horizontal contact line, allows using points along the whole profile of the drop. So it is much less affected by the spot of reflected light seen on left side in Fig. 7.

A further check was done for images of drops on a strongly hydrophilic substrate, with contact angles less than 10°. The proposed method gives realistic values (6.9° at left and 7.1° at right), as shown in Fig. 9 while the software provided by manufacturer failed to calculate the contact angle on both sides.

The position of contact line used in calculations was the one estimated by the manufacturer software. The boxes (a, b) show the result of edge detection done by manufacturer's software (a) and with proposed method (b). The upper-right corners of boxes contain a zoomed part of the image, close to the contact line of the drop and explain the cause of failure. This is called corner erosion [20] and for drop images appears in points where drop profile presents cusps. It can be reduced by using thresholds adjusted locally. Given the scarcity of information provided by equipment manufacturers about the algorithms used in the software provided with apparatus, it is difficult to elaborate more about this failure.

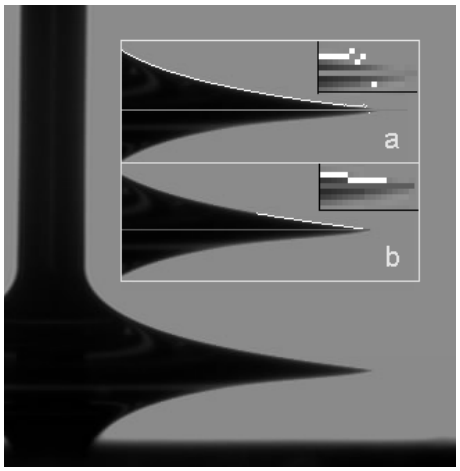

Fig. 9 – Behavior of edge detection algorithms near a cusp on drop profile. Inserts:
a) – commercial software; b) – proposed method.

Summarizing, if one can control the collimation of back-lighting, SVED is preferable for measuring of the contact angles, as unbiased and with smaller errors. In cases when back-lighting is deficient or the shape of droplet produces strong reflection spots nearby its edges on image, as *e.g.* for drops with very low contact angles, the method proposed in this paper is more stable and gives values for contact angles close to reality although with bigger errors than standard software used in commercial instruments.

5. CONCLUSIONS

Various factors are considered, that influence the quality of images produced by contact angle goniometers. This analysis provides guidelines for choosing hardware settings that lead to images and contact angle measurements of better quality. One shows the influence back-light rays reflected from drop surface on the brightness profile of drop image and how to account for it.

Alternatively, understanding the influence of these factors for images kept in less than optimal conditions, one can devise adapted algorithms for determination of contact angles that are less affected and more stable in processing of such images. This may be important when studying the time and/or position dependence of advancing and receding contact angles by pumping the drop, while keeping to a minimum the number of rejected frames or said differently, the time evolution information.

In cases when back-lighting is inappropriate or a particular droplet shape produces strong reflection spots nearby its edges on image, the proposed method is more stable and gives values for contact angles close to reality. The method is also valuable in the case of low contact angles ($< 10^{o}$) when reflection spots on drop image are more probable.

Acknowledgments. The financial support of the Romanian Ministry of Education and Research (Project COMAFI III PN09-45 of CORE Program) is gratefully acknowledged. Author thanks Drs. T. Beica and L. Frunza for many useful discussions and Prof. N. McMillan for constructive criticism that stimulated an improved argumentation.

REFERENCES

1. A. I. Rusanov, V. A. Prokhorov, *Interfacial Tensiometry,* Elsevier, Amsterdam, 1996.
2. N. D. McMillan, V. Lawlor, M. Baker and S. Smith, *Drops and Bubbles in Interfacial Research,* Elsevier, 1998.
3. M. Hoorfar, A. W. Newmann, Adv. Colloid Interfac., **121**, 25–49 (2006).
4. J. Canny, IEEE Trans. Pattern Anal., **8**, 679–698 (1986).
5. Q. Song, G. Zhang and Z. Qiu, Instrum. Sci. Technol., **22**, *4*, 375–395 (2003).
6. M. G. Cabezas, J. M. Montanero and C. Ferrera, Meas. Sci. Technol., **18**, 1637–1650 (2007).

7. J. F. Gomez-Lopera, J. Martìnez-Aroza, A. M. Robles-Pèrez and R. Roman-Roldan, J. Math. Imaging Vis.**,** **13**, 35–56 (2000).
8. F. van der Heijden, *Image Based Measurement Systems*, J. Wiley & Sons Chichester, 1995.
9. T. Klinger, *Image processing with LabVIEW and IMAQ Vision*, Prentice Hall, New Jersey, 2003.
10. K. Thurow, T. Kruger and N. Stoll, J. Autom. Method Manag., 1–10 (2009).
11. V. H. Chhasatia, A. S. Joshi and Y. Sun, Appl. Phys. Lett., **97**, 231909 (2010).
12. Y. L. Hung, Y. Y. Chang, M. J. Wang and S. Y. Lin, Rev. Sci. Instrum., **81**, 065105 (2010).
13. F. K. Hansen, G. Rodsrud, J. Colloid Interf. Sci., **141**, 1–9 (1991).
14. L. Busoni, M. Carlà, L. Lanzi, Rev. Sci. Instrum., **72**, *6*, 2784–2791 (2001).
15. J. R. Saylor, N. A. Sivasubramanian, Appl. Optics, **46**, 5352–5367 (2007).
16. A. M. Emelyanenko, L. B. Boinovich, Instrum. Exp. Tech., **45**, 44 – 49 (2002).
17. M. Born, E. Wolf, *Principles of Optics*, 7-th ed. Cambridge University Press, 2003.
18. Yu. A. Lemeshko, Yu. V. Chugui and A. K. Yarovaya, Optoel. Instrument. Data Processing, **43**, 284–291 (2007).
19. F. van der Heijden, IEEE Trans. Pattern Anal. Mach. Intell., **17**, 16–33 (1995).
20. H. K. Huang, *PACS and Imaging Informatics*, 2nd ed., Willey-Blackwell, Hoboken, New Jersey, 2010.
21. E. H. Barney Smith, *16th European Signal Processing Conference (EUSIPCO)*, Lausanne, 2008.
22. Y. Y. Zuo, M. Ding, A. Bateni, M. Hoorfar and A. W. Neumann, Colloid Surface, A **250,** 233–246 (2004).